Sine wave electropermeabilization reveals the frequency-dependent response of the biological membranes

Tomás García-Sánchez*, Caterina Merla, Jessica Fontaine, Adeline Muscat, Lluis M. Mir

Vectorology and Anticancer Therapies, UMR 8203, CNRS, Univ. Paris-Sud, Gustave Roussy, Université Paris-Saclay, 94805 Villejuif, France

A B S T R A C T

The permeabilization of biological membranes by electric fields, known as electroporation, has been traditionally performed with square electric pulses. These signals distribute the energy applied to cells in a wide frequency band. This paper investigates the use of sine waves, which are narrow band signals, to provoke electropermeabilization and the frequency dependence of this phenomenon.

Single bursts of sine waves at different frequencies in the range from 8 kHz–130 kHz were applied to cells in vitro. Electroporation was studied in the plasma membrane and the internal organelles membrane using calcium as a permeabilization marker. Additionally, a double-shell electrical model was simulated to give a theoretical framework to our results.

The electroporation efficiency shows a low pass filter frequency dependence for both the plasma membrane and the internal organelles membrane. The mismatch between the theoretical response and the observed behavior for the internal organelles membrane is explained by a two-step permeabilization process: first the permeabilization of the external membrane and afterwards that of the internal membranes. The simulations in the model confirm this two-step hypothesis when a variable plasma membrane conductivity is considered in the analysis.

This study demonstrates how the use of narrow-band signals as sine waves is a suitable method to perform electroporation in a controlled manner. We suggest that the use of this type of signals could bring a simplification in the investigations of the very complex phenomenon of electroporation, thus representing an interesting option in future fundamental studies.

1. Introduction

The interaction of the cell membrane with high intensity pulsed electric fields is widely used to provoke the transient permeabilization of the cell membrane in a phenomenon termed electroporation, also known as electropermeabilization. This is routinely used as a technique to incorporate membrane-impermeant molecules into the cell. The most relevant medical applications use this technique in combination with chemotherapeutic agents (Electrochemotherapy) [1–3] or DNA plasmids (Electrogenetherapy) [4,5]. Furthermore, when the effect of the electric field causes cell death the phenomenon is called Irreversible Electroporation and it is used for tissue ablation or microbial deactivation among other applications [6–9].

Electropermeabilization results from the interaction of biological membranes with an electric field, but it is not the only possible outcome of this interaction. It is widely known that the electric field and the cell membrane can interact by thermal or non-thermal mechanisms producing effects other than electroporation, depending on the

characteristics of the applied electric field [10]. Apart from the evident thermal effects, direct electrical forces on cells by dipole interactions, mechanical stress, electrophoretic movements, changes in conformational state of proteins, etc. have been deeply described [11–13]. These effects depend mainly on the frequency and amplitude of the applied electric field. Moreover, the electrodes, another important part of the system, are also influenced and modified by the electric field. The events at the electrodes such as bubble gas formation, metallic ion release, pH changes, etc. [14–16] are also dependent on the frequency of the applied electric field and on the current that flows through them [17].

In this context of complexity, the reader can understand how any attempt of simplification in the electroporation phenomenon must be considered as a step forward in the understanding of its mechanisms. Similar to studies where the complexity of the cell membrane was reduced by using artificial lipid bilayers [18–20], it seems reasonable to reduce the complexity of the electric field applied to cells. Regarding the type of signals used, electroporation has traditionally made use of

---

short square direct current (DC) electric pulses to modify cell membrane properties. Although the duration of these square pulses can range from nanoseconds to milliseconds, unipolar pulses of 100 μs are the most utilized, especially for clinical applications [21,22]. A square waveform is a broadband signal whose energy content is distributed in the frequency domain from DC to a cutoff frequency dependent on the duration of the square pulses, this implies a complex spectrum. On the contrary, the use of alternating current (AC) signals with simple spectral content, like the sine wave signals, should represent a much better option, especially if the goal is to verify if different frequency components of the electric field have overlapped effects on the cell membrane during electroporation. This latter assumption is yet to be demonstrated but would justify the suitability of these signals as a simpler framework of study.

Although theoretically described [23–25], few experimental reports have deeply studied the ability of AC signals to cause cell permeabilization [26–28]. For example, efficient gene transfer and cell fusion was accomplished by superposition of a radiofrequency field and a DC pulse [29,30], or more recently, the use of high frequency bursts of bipolar square pulses has been deeply studied for tissue ablation by irreversible electroporation [31,32]. Also, many theoretical descriptions have predicted the dependency of electroporation on the frequency of the applied electric field based on the calculation of the induced transmembrane potential according to Schwan equation [33–35]. Surprisingly, as far as the authors know, only one study could clearly show the frequency dependence of electroporation in the frequency band from 0.1 to 300 kHz using sine signals [36]. In that work, the frequency dependence was demonstrated by the increase in the threshold electric field intensity for electroporation with increasing frequency. On the contrary, another study using also sine signals showed controversial results revealing no dependence of electropermeabilization on the AC frequency in the range of 20–160 kHz [27]. Also cell electrofusion revealed a frequency dependence not in accordance with theoretical predictions [30]. Finally, the frequency dependence on the interaction of the electric field, not only with the plasma membrane, but also with the internal structures has been the basis for many studies where the goal was the manipulation the internal organelles [26,37–39].

In the present work, the dependence on electropermeabilization efficacy with the frequency of the electric field was studied using single bursts of pure sine signals. The narrow-band applied electric fields were in the frequency range from tens to hundreds of kHz. The permeabilization of both plasma membrane and the membrane of internal organelles was studied using calcium as a permeabilization indicator. Calcium has been used by many research groups as a sensitive method to detect permeabilization of both internal and external membranes [40,41]. The interest of using this small molecule is that even small amounts entering the cells can trigger a large response amplified by physiological processes of the cell, such as the calcium-induced calcium-release (CICR), thus allowing to have a very sensitive method. Also, its use is very interesting when studying the possible permeabilization of intracellular structures as it is naturally present in high concentration inside internal organelles such as the endoplasmic reticulum. However, there is some controversy in its use because it has been demonstrated that other processes could also result in the release of calcium in the cell cytosol. Thus care must be taken in the interpretation of the results [42]. Additionally, bipolar square pulses were also used for comparison. Our results were supported by theoretical simulations of the frequency dependent values of the induced transmembrane potential in the plasma membrane and the internal organelles using a double shell model.

2. Materials and methods

2.1. Cells and chemicals

Chinese hamster lung cell line DC-3F was grown in complete

medium which consisted in MEM-Minimum Essential Medium (Life Technologies, Saint Aubin, France) supplemented by 10% fetal bovine serum (Life Technologies) and antibiotics (500 U/ml penicillin, and 500 μg/ml streptomycin). Cells were maintained in a humidified atmosphere at 37 °C and 5% CO_2 and routinely sub-cultured every two days.

Four hours before the experiments, cells were trypsinized, centrifuged and resuspended in normal culture medium at a concentration of 500×10^3 cells/ml. Afterwards, cells were seeded on glass coverslips (11×32 mm) in order to allow them to slightly attach to the coverslip surface while maintaining their spherical shape.

Fluo-4 AM (λex = 496 nm, λem = 515 nm) which is a fluorescent calcium marker was used as a probe to visualize the variations in the cytosolic calcium concentration as a result of membrane permeabilization. This probe increases its fluorescence > 100 fold upon binding to calcium. Previous to experiments, cells were incubated for 30 min with 5 μM Fluo-4 AM in complete MEM culture medium in a humidified atmosphere at 37 °C and 5% CO_2. Subsequently, the coverslips were washed with PBS (Phosphate Buffered Saline), and the culture medium was replaced by a low conductive electroporation buffer containing 250 mM Sucrose, 1 mM $MgCl_2$, 6 mM Hepes (pH = 7, σ = 0.1 S/m). The use of a low conductivity buffer ensured the minimization of some undesired effects such as electrolytic reactions at the electrodes and heating by Joule effect. This last was negligible (≈ 0.17 °C) under the applied conditions. Additionally, the use of a low conductivity buffer was motivated to avoid any current limitation of the pulse amplification system.

Two different conditions were used to study either the electropermeabilization of the plasma membrane or the permeabilization of the membrane of the internal organelles, namely the endoplasmic reticulum. In the first condition, a high concentration of Ca^{2+} was added to the extracellular buffer (the low conductive buffer was supplemented with 4 mM Ca^{2+}). Thus, an increase in Fluo-4 fluorescence would be mainly the result of Ca^{2+} influx from the external medium. In the second condition, the concentration of calcium in the extracellular space was kept to zero so that an increase in fluorescence can only be detected if calcium is released through the permeabilized membrane of the internal organelles. Particularly, the electropermeabilization of the endoplasmic reticulum, which constitutes the most important store of intracellular calcium, can be detected. In this second condition the low conductive buffer was supplemented with 2 mM (final concentration) of EGTA (ethylene glycol tetraacetic acid) which is a calcium chelator that traps any calcium ion present in the buffer ensuring that no calcium can enter the cell from the extracellular space.

2.2. Experimental setup

In order to expose the cells to a sinusoidal electric field of the desired frequency, amplitude and duration, a custom exposure system was developed. In particular, a custom-made amplifier based on the power operational amplifier PA96 (Apex Microtechnology, Tucson, AZ) was designed and built. The signals at the input of the amplifier were synthetized by an arbitrary waveform generator (Agilent 33250A) controlled by a custom LabVIEW program (National Instruments, Inc., Austin, TX) which allowed to control by software the shape of the signal, its amplitude, duration and frequency (see schematic of the setup in Fig. 1).

The amplified signals at the output of the amplifier were connected to the electric field exposure system which consisted in a glass slide with two parallel thick gold electrodes deposited on its surface. The electrodes had a thickness of 25 μm and were separated by a gap of 300 μm between them (see details in Fig. 1). The system was adapted from the device presented in detail in Dalmay et al. [43].

According to the theory of the dielectric relaxation of biological tissues, we presumed that any change in the response of cell membrane to the electric field should occur in the range between a few kHz and
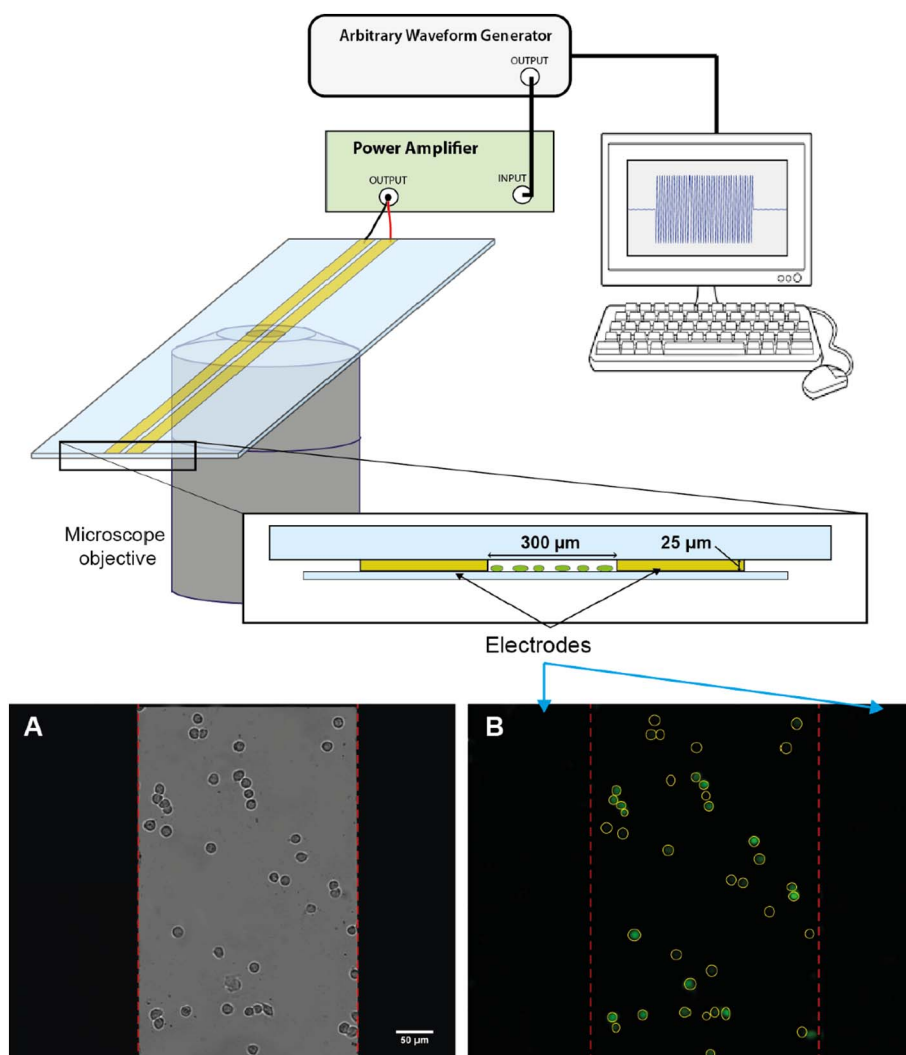
Fig. 1. Upper panel: Schematic representation of the experimental setup. The output of the arbitrary waveform generator is connected to a custom-made amplifier. A glass coverslip containing attached spherical cells was placed on top of the channel gold electrodes and turned upside down before being inserted in the microscope stage. Bottom panel: Representative brightfield (A) and fluorescent micrographs of the cells in the channel and the mask used for quantification (B).

some hundreds of kHz. In previous experiments (data not shown), starting at few kHz, a complete loss of efficacy was observed for frequencies above 200 kHz. In further studies we decided to limit the range to 7 logarithmically separated points starting at some kHz and ending below 200 kHz. The frequencies of the sine signals used for the experiments spanned from 8 kHz up to 130 kHz logarithmically equidistributed following Eq. (1). Single sinusoidal bursts were applied to cells with durations of either 2 ms or 5 ms and electric field peak intensity (E_{peak}) of 500 V/cm or 600 V/cm.

$$\text{freq }(n)_{(n=1,\dots7)} = \frac{10^{(4.5+0.2\times n)}}{2\pi}\text{Hz} \tag{1}$$

Additionally, equivalent bipolar square pulses with the same duration were applied for comparison. In order to have equivalent conditions in terms of energy applied to the samples, we decided to apply the concept of Root Mean Square (RMS) value to calculate the corresponding amplitudes for the square pulses. For a sinusoidal current, the RMS value is equal to the value of the direct current that would produce the same average power dissipation in a resistive load and can be calculated following Eq. (2) (refer to Fig. 2 center insert).

$$V_{RMS} = \sqrt{\int_0^T \frac{1}{T}V_{peak}^2 \sin^2(\omega t)dt} = \frac{V_{peak}}{\sqrt{2}} \tag{2}$$

where V_{peak} is the peak amplitude of the sine wave, and T is the period

of the signal. Accordingly, the amplitudes of the bipolar square pulses used for comparison were reduced by a $\sqrt{2}$ factor with respect to its corresponding sinusoidal equivalent. It is important to note that due to the inversing polarity of a sinusoidal signal, it was considered more correct to use bipolar pulses in the case of the square signals. The square pulses were also generated using the same arbitrary waveform generator and amplifier architecture previously described. The generated waveforms were acquired with a digital oscilloscope (LeCroy WaveMaster 808Zi). In Fig. 2 two temporal recordings of both sine and square signals are shown as an example.

2.3. Imaging and post-processing

Just before the electric field exposure, the coverslips containing the cells were placed on the top of the microchamber that had been previously filled with low conductive buffer, cells being thus located inside the channel. The whole exposure system was turned upside down and placed in the stage of an inverted fluorescence microscope (Observer Z1, Zeiss, Germany) with 40 X magnification for the real time observation of cytosolic calcium concentration variations (refer to Fig. 1). Images of cells were taken every 5 s with a Zeiss AxioCam Hrc camera for 10 s immediately before, and for 5 min immediately after the electric field delivery.
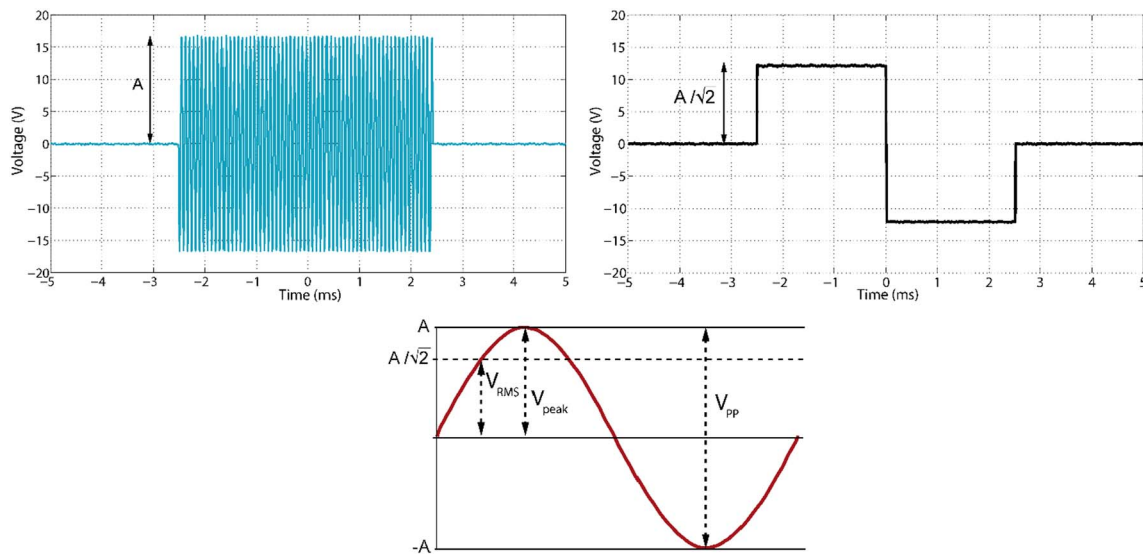
Fig. 2. Example of the temporal recordings of the sine (left upper panel) and bipolar square (right upper panel) waves used in experiments. Lower insert shows the relation between the peak (V_{peak}), peak to peak (V_{pp}) and RMS (V_{RMS}) amplitudes defined in a sine wave.

Sequential images were post-processed with ImageJ software and the variations in fluorescence intensity were automatically quantified for each individual cell. Further processing performed in MATLAB (Mathworks Inc.) allowed the determination of the percentage of cells displaying a calcium spike. This percentage was calculated as the fraction of cells exceeding a fluorescence threshold after the electric field delivery. Moreover, for each cell over the threshold the automatic system checked for the shape of the fluorescence variation. Only cells whose maximum in fluorescent was present in the first minute after pulse application (spike or stepped-shaped response) were positively counted. Between 25 and 45 cells on average were analyzed for each experimental point. Additionally, the Area Under the Curve (AUC) was quantified for each individual calcium spike.

2.4. Simulations

Calculations of the induced transmembrane potential (iTMP) were performed using a single cell model based on a spherical multilayered structure [44,45]. Briefly, the model computed the iTMP for both the plasma membrane and the membrane of an internal concentric organelle (i.e. the endoplasmic reticulum ER). The cell model was composed by the inside content of the organelle, the membrane of the organelle, the cell cytoplasm, the plasma membrane, and the extracellular medium considered as separate compartments (see Fig. 3). The geometric details of the cell and the electrical characteristics of each compartment are reported in Fig. 3. Realistic cell dimensions were assessed from confocal microscope images of DC-3F cells (data not shown).

The permittivity of the extracellular medium, cell cytoplasm and internal organelle were fixed as saline solutions as specified in [34,44]. The conductivity of the extracellular medium was fixed to the measured values of the cell suspending buffer. The rest of values were chosen in the range suggested in Kotnik et al. [23] and Merla et al. [46] (see values in Fig. 3). Specifically, for the conductivity of the internal organelle membranes, the value reported in [23] was taken into account, while for the plasma membrane we used values experimentally assessed for the membranes of liposomes (constituted by phospholipid double layers) as reported in [46]. Finally, to simulate the changes in the plasma membrane during electroporation, simulations have been carried out using increasing membrane conductivity values. These values were fixed in the range according to the current literature to a non-electroporated and an electroporated membrane respectively [47].
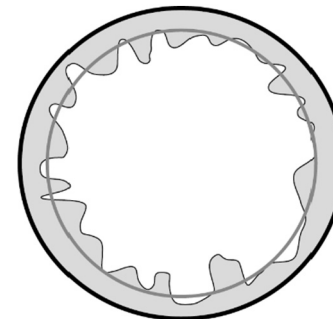
Plasma membrane ━	Organelle membrane ━
- thickness = 5 nm	- thickness = 3.5 nm
- $\sigma_m = 1 \times 10^{-7}$ - 1×10^{-2} S/m	- $\sigma_{IN} = 3 \times 10^{-7}$ S/m
- $\varepsilon_r = 12.7$	- $\varepsilon_r = 18.6$
Cytoplasm ▢	**Organelle inside** ▢
- Radius = 13 μm	- Radius = 12 μm
- $\sigma_c = 0.4$ S/m	- $\sigma_o = 0.6$ S/m
- $\varepsilon_r = 72.3$	- $\varepsilon_r = 72.3$

Fig. 3. Details in the double shell model used in the simulations.

The EM computation was performed under the assumption of quasi-static conditions. In spherical and spheroidal cell domains, it is possible to solve the Laplace equation as explained in [48] and implemented in [44,49] including a Debye description of cell compartments (using home-made routines implemented in MATLAB). The uniqueness of the EM solution is guaranteed by the associated boundary conditions assuring the continuity of the potential between the different cell compartments as well as the conservation of the normal component of the field at these interfaces. The extracellular electric field was fixed to the applied value of 600 V/cm. In order to simulate the frequency response of the induced TMP, a wideband study from DC up to 10 MHz was performed.
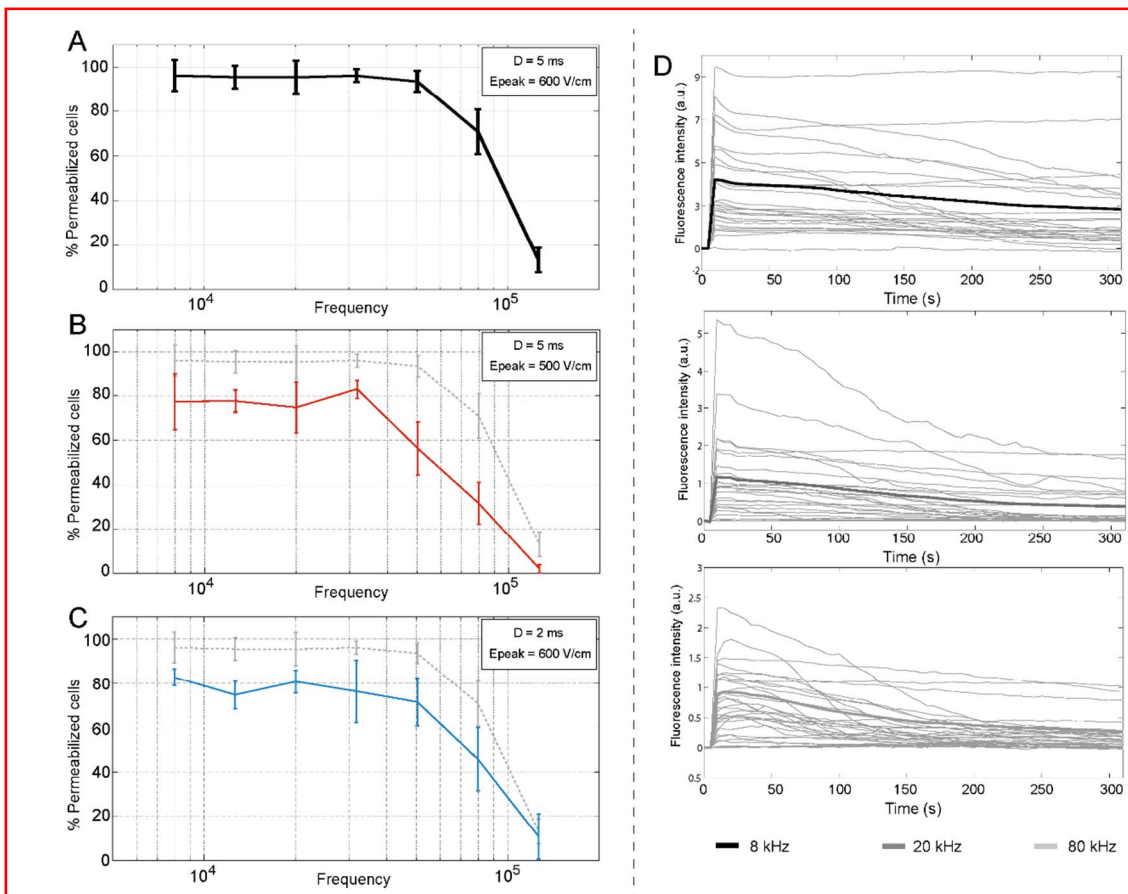
Fig. 4. Plasma membrane permeabilization rates obtained for the sinusoidal exposure at the different frequencies assayed (with 4 mM extracellular Ca^{2+}). A) A single burst of 5 ms and $E_{peak} = 600$ V/cm or $E_{peak} = 500$ V/cm was applied in panels A and B, respectively. C) A single burst of 2 ms and $E_{peak} = 600$ V/cm was used. Dotted line in B and C reproduces the results in A for comparison. A minimum of $n = 3$ experiments performed at least in two different days are pooled together. Error bars correspond to $\pm$ SD (standard deviation). Between 25 and 45 cells were analyzed in each experiment. D) Examples of the time courses in fluorescence for the conditions shown in A. From top to bottom, data correspond to an applied frequency of 8 kHz, 20 kHz and 80 kHz.

3. Results and discussion

3.1. Permeabilization of plasma membrane

As explained in Section 2.1, for this set of experiments the extracellular low conductivity buffer was supplemented with calcium so that the detection of a calcium spike responds to the influx of calcium from the extracellular space resulting from the permeabilization of the cell membrane. A cell was counted as positively permeabilized as long as its fluorescence exceeded a certain threshold after pulse application. Additionally, only cells whose fluorescence reached a maximum after pulse application were considered permeabilized. Fig. 4A, B and C show the percentages of permeabilization obtained for three different pulsing conditions using sine waveforms of different frequencies. A minimum of $n = 3$ experiments performed at least in two different days are pooled together. Error bars correspond to $\pm$ SD (standard deviation). Between 25 and 45 cells were analyzed in each experiment.

In Fig. 4A a single sinusoidal burst of 5 ms duration and E_{peak} of 600 V/cm was applied with the different frequencies under study. The results show how the percentage of permeabilized cells displays a plateau in the low frequency band (up to 50 kHz) where almost all cells are permeabilized (mean value of around 95%). This percentage drastically decreases with frequency and the efficiency of electroporation is zero for frequencies above 130 kHz. Additional tests performed at a frequency of 200 kHz showed persistently zero % of cells permeabilized (results not shown).

In Fig. 4B similar data are shown but with a lower electric field intensity applied ($E_{peak} = 500$ V/cm). As expected, the percentage of

electropermeabilized cells is reduced as the intensity of the electric field decreases. For cells exposed to frequencies below 50 Hz, about a 20% of reduction in the percentage of permeabilized cells is measured with respect to the previous case. Under this condition, the decay in the permeabilizing efficacy of the sinusoidal field becomes significant already at 50 kHz. However, on average, the frequency response is similar to the previous condition since dotted (previous condition) and solid lines keep an overall parallelism.

Data in Fig. 4C correspond to experiments where the duration of the electric field exposure was reduced to 2 ms while maintaining an electric field E_{peak} of 600 V/cm. Similar to the previous case, the number of permeabilized cells is lower than in the first condition. Around a 20% reduction is quantified. In this situation the frequency behavior stays fully in agreement with the first results; the plateau in the efficacy of the electric field is maintained constant until a frequency of 50 kHz and is significantly reduced for frequencies above.

In order to confirm that a saturation effect in the frequency response may exist, meaning that even if the energy delivered to cells is further increased, there exists a loss of efficiency of electric field for the high frequencies, supplementary experiments with a burst duration of 100 ms and E_{peak} of 600 V/cm were performed (see Supplementary Fig. S1A). These results show that there is indeed such a saturation phenomenon and even increasing the duration of pulses by 20 fold, a similar frequency response is obtained. This observation confirms that, independently of the amount of energy delivered to the cells, electroporation only takes place if the interaction of the oscillatory electric field with the plasma membrane is effective.

Additionally, we can ensure that the chosen parameters for
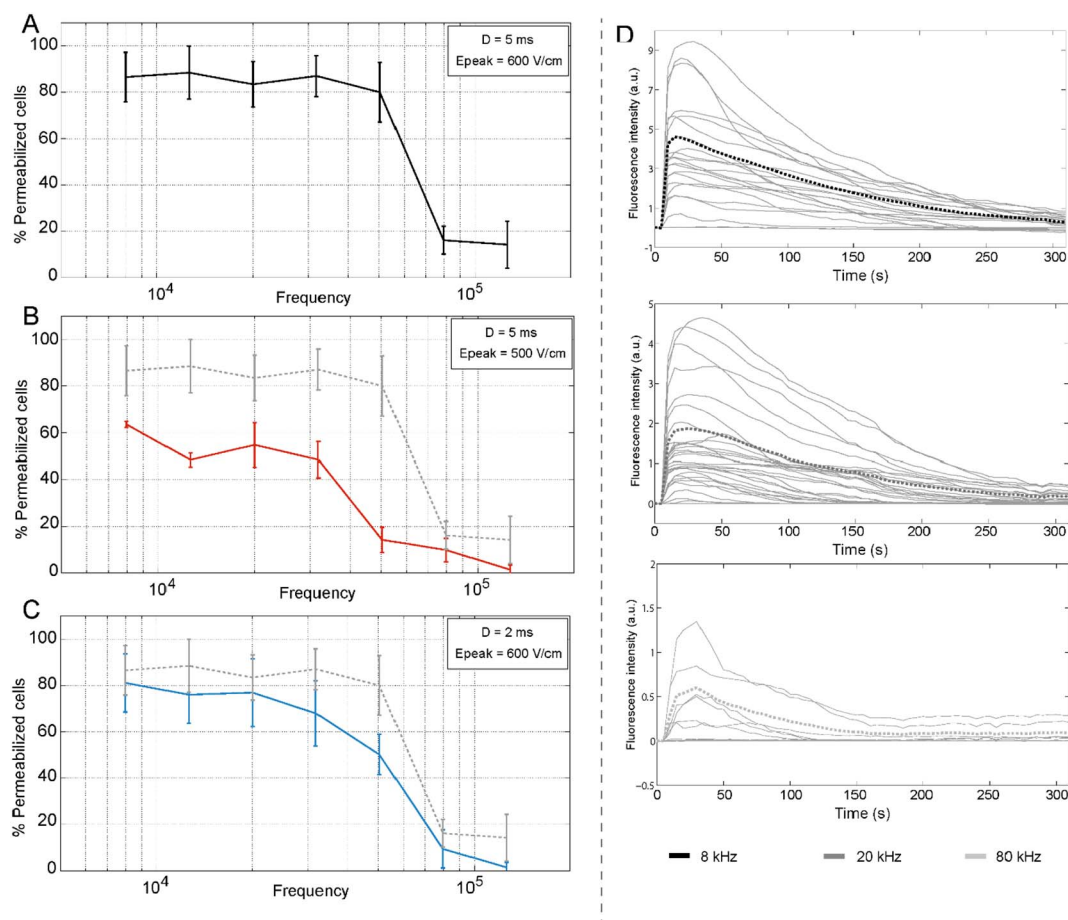
Fig. 5. Rates of cells displaying a calcium peak obtained for the sinusoidal exposure at the different frequencies assayed (extracellular calcium concentration ≈ 0 mM). A) A single burst of 5 ms and E_{peak} = 600 V/cm or E_{peak} = 500 V/cm was applied in panels A and B, respectively. C) A single burst of 2 ms and E_{peak} = 600 V/cm was used. Dotted line in B and C reproduces the results in A for comparison. D) Examples of the time courses in fluorescence for the condition in A, from top to bottom, 8 kHz, 20 kHz and 80 kHz.

duration, and amplitude of the electric field are near to the optimal maximum permeabilization efficiency for these experimental conditions. As observed, a slight reduction in the amplitude or duration of the applied burst has an immediate effect in the decrease of electroporation occurrence, meaning that the field applied to cells is not excessive. Furthermore, the time courses in the variation of cytosolic calcium concentration (see examples in Fig. 4D) also suggest that the electric field application is not causing massive disruption of plasma membrane. As shown, the cells are able to pump out the excess of calcium from the cytoplasm accumulated after electropermeabilization suggesting that the plasma membrane can recover after pulses. However, the same type of data corresponding to much longer exposure times (see Supplementary S1B) suggest that irreversible damage to cell membrane maybe caused in the low frequency band under these more drastic conditions.

Additionally, previous data from our team allow us to ensure that the increase of cytosolic calcium coming from the extracellular space is not due to the activation of voltage operated calcium channels (VOCC's) in the plasma membrane [50]. This family of channels, activated by membrane depolarization, would lead to calcium entry due to an increase in the transmembrane potential. Although these channels are numerous in electrically excitable cells they can be also found in other cell types. According to our previous study, using traditional 100 μs high intensity square pulses the inhibition of these channels did not affect the occurrence of calcium spikes after the electric pulses confirming that they are not implied in the increased entry of calcium from the external buffer.

These first results confirm the ability of sinusoidal electric fields to

cause successful permeabilization of the plasma membrane in the studied frequency range. As predicted by the theory, the frequency dependence in the electroporation efficiency for a sinusoidal field follows a low pass filter behavior [23,25,35,36,51]. At low frequency, the lipid bilayer has a low ionic permeability and is considered a thin insulating shell surrounded by ionic solutions. In this situation, cell membrane is polarized and an induced transmembrane potential (iTMP) rises upon electric field exposure. Starting from frequencies in the kHz range capacitive coupling allows the electric field penetrating the intracellular space and at sufficiently high frequency, the current can freely flow through the membrane, what results in the abolishment of the iTMP. This explanation is in agreement with the classical electroporation models that consider electroporation as a membrane charging-dependent phenomenon [52–54]. At sufficiently high frequencies negligible net ionic charge accumulates at both sides of the membrane leading to a situation where electroporation is no longer possible.

However, depending on the intrinsic parameters of a specific biological system, such as the extracellular and intracellular conductivities, membrane capacitance, cell radius, etc., the charging time and thus the frequency response of the cells can be different [45]. This is perfectly reflected in the measurement of the dielectric parameters of different biological tissues in the frequency domain. In the radio frequency band, around the so-called β dispersion (usually from 1 kHz to 1 MHz) the frequency behavior of different tissues has shown clear differences [55,56].

3.2. Intracellular effects

In the following set of experiments, calcium was eliminated from the extracellular buffer by addition of a calcium chelator (EGTA). In this way, the presence of a calcium spike in the cytoplasm would necessarily result from a release from the internal organelles where calcium is stored, mainly the endoplasmic reticulum (ER), which constitutes the most important internal store of calcium [57]. Previous studies applying nanosecond electric pulses already demonstrated that the intracellular calcium mobilized after electric field exposure mainly came from ER [41,58]. A recent study performed in DC-3F cell line and similar experimental conditions to this study showed that if ER stores were depleted using thapsigargin, 100 μs pulses did not provoke a calcium spike in the absence of extracellular calcium [50]. Equivalent exposure conditions to the ones used in Section 3.1 were applied in this new set of experiments. In Fig. 5A, B and C the percentages of peak positive cells are depicted for each condition and in Fig. 5D the time evolution of the intracellular calcium concentration for 5 min after pulse application is also shown for the same three example frequencies that in the previous set of experiments.

As observed, the frequency response in this set of experiments displays again a low pass filter behavior. For a burst of 5 ms and E_{peak} = 600 V/cm the obtained percentages are constant and around 85% in the low frequency band up to 50 kHz; subsequently this percentage reduces rapidly for higher frequencies to < 20%. For the condition where the electric field intensity is reduced to E_{peak} = 500 V/cm this percentage stays around 55% for frequencies below 30 kHz and reduces drastically for the frequencies above. In the last condition (Fig. 5C), corresponding to a reduction in the burst duration to 2 ms, the obtained values are around 75% up to 50 kHz and reduce for higher frequencies.

As shown in Fig. 5B, when the amplitude of the electric field is reduced from 600 to 500 V/cm, there is a reduction of around 30% in the percentages obtained in the low frequency band. On the contrary, when duration is reduced instead, (from 5 to 2 ms, Fig. 5C), the decrease in the number of cells displaying a calcium spike is only around 10% on average. This suggests that, for the chosen parameters, there is a much stronger dependence on the intensity of the electric field. This dependency is also displayed at high frequency. In the first (5 ms–600 V/cm) and last (2 ms–600 V/cm) conditions, the rates stay similar up to 50 kHz and they drastically decrease at 80 kHz. By contrast, the corresponding result for the condition in Fig. 5B, where amplitude was reduced to 500 V/cm, shows that the most significant decrease in efficacy takes place at a lower frequency, 50 kHz instead of 80 kHz.

These experiments suggest the ability of sinusoidal waves to cause permeabilization also of the internal cell stores with similar parameters than those needed to permeabilize the external membrane. However, although this is the most plausible explanation, there are controversial results trying to elucidate if the increase of intracellular calcium when cells are exposed to a permeabilizing electric field in free calcium buffers is a direct reflect of reticulum permeabilization, or if it is the consequence of an indirect release of calcium caused by cell signaling. It has been recently demonstrated that a mechanism for nsEP-induced release of intracellular Ca^{2+} is the generation of inositol trisphosphate (IP$_3$) in the cytoplasm after phosphatidylinositol 4,5-bisphosphate (PIP$_2$) hydrolysis which triggers the release of calcium from the ER [59]. However, other studies demonstrated that, even when the calcium induced-calcium release (CIRC) IP$_3$R receptors were blocked, a release of calcium from the ER was still detected using also nanosecond pulses [41]. Another recent study confirmed the electropermeabilization of inner membranes by using inhibitors for IP$_3$R and ryanodine receptors (RyRs) and using 100 μs pulses [50]. Although these studies support the idea of internal membranes permeabilization, and the results of the present study are also compatible with it, we cannot however reject the possibility of an additional signaling pathway for the obtained increase in intracellular calcium detected.

Finally, the examples for the evolution of the cytosolic calcium concentration at three different frequencies shown in Fig. 5D compared to the experiments in the presence of extracellular calcium (Fig. 4D) display some differences. Although the dynamics are similar, it can be noticed that at 8 and 20 kHz the maximum in fluorescence under the presence of extracellular calcium is displayed immediately after pulse, while in the conditions without calcium the fluorescence increases for about 20 s after exposure. This observation is less evident at 80 kHz. As discussed above, we cannot reject the possibility of an indirect signaling mechanism implied in the release of extracellular calcium that could be responsible for this difference. However, in other previous studies, where the major calcium channels were inhibited, Ca^{2+} rise dynamics were indeed different and dependent on the level of permeabilization and the source of Ca^{2+} (extracellular or intracellular) [60]. The observed difference could be explained because in the experiments with extracellular Ca^{2+}, there are two different sources supplying calcium to the cytosol (extra/intra cellular reservoirs). Additionally, in the extracellular compartment the availability of calcium and the concentration gradient are much higher than in the reticulum. These reasons explain a faster diffusion of Ca^{2+} to the cytosol from the extracellular space through the plasma membrane.

Considering our results as a reflect of electropermeabilization of the internal membranes, the observed low pass filter frequency response is not in agreement with the theoretical predictions where a band pass filter behavior is usually assigned for the intracellular membranes [23,24]. The mismatch found between our observations and the theory is discussed in detail in Section 3.5.

3.3. Area under the curve

An alternative analysis is presented in this section to give a qualitative idea of the changes in the extent of permeabilization with frequency. During the analysis of the data it was noticed that, for increasing frequencies, not only less cells were permeabilized but also that, the dynamics in the evolution of the fluorescence after pulse were different (lower amplitude of the fluorescence peak and shorter time to return to the fluorescence basal level). This was observed even for frequencies where the obtained rate of permeabilization was similar. To account for this observation, the Area Under the Curve (AUC) for each calcium spike detected was measured. Although maybe obvious, it is important to emphasize that this quantification was only performed in cells that displayed a calcium spike, i.e. cells that were permeabilized.

AUC measurement combines the complementary information about the initial amplitude of the calcium spike and the temporal evolution of the decrease of calcium in the cytoplasm. In Fig. 6A an example for the measured area is shown for both sets of experiments (with or without calcium in the extracellular buffer). It must be emphasized that the use of Fluo-4 AM molecule, which is a non-ratiometric calcium indicator, does not allow the calculation of the real calcium concentration and thus, the information provided by this parameter should be taken just in a qualitative way.

Fig. 6B and C depict the frequency dependence of the AUC for the same conditions shown in the previous sections. As observed, a monotonous decrease with increasing frequency is obtained in all cases. It is interesting to notice the similarity in the values obtained for the two conditions corresponding to an applied E_{peak} of 600 V/cm and different durations (5 and 2 ms) while the condition where E_{peak} = 500 V/cm provides always lower values. In contrast to the results previously shown, the plateau in the lower frequency band is no longer present in this analysis. This difference can be explained based on the fact that the information provided by the rates of permeabilization is binary, since only two possible states of permeabilization are possible (permeabilized or not). On the contrary, the AUC estimation provides a more gradual qualitative idea of the permeabilization extent. When cells are less permeabilized, they display lower amplitude calcium peaks and additionally these peaks are shorter in duration. These
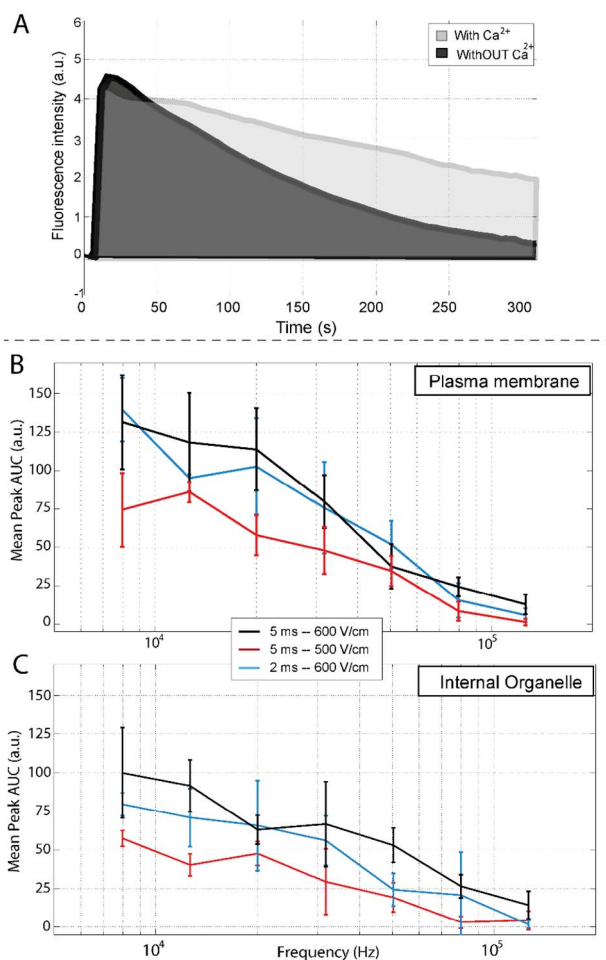
Fig. 6. Area under the Curve quantification. A) Example of the measured area for two experimental curves (with and without calcium). B and C) Frequency dependence in the AUC for experiments corresponding to the three exposure conditions assayed. Panel B shows the results corresponding to experiments performed in presence of extracellular calcium, in panel C extracellular calcium was completely eliminated.

results suggest that, in fact, in the frequency range under study, the higher the frequency, the lower the effect of the electric field.

Additionally, comparing Fig. 6B and C, a lower AUC is systematically obtained for experiments where the only possible source of calcium are the internal stores. This could be explained based on different considerations. First, as discussed above, in the presence of extracellular calcium, we should expect a higher amount of calcium diffusing to the cytoplasm from a very large reservoir, the external medium. Moreover, in these experiments the calcium detected in the cytoplasm emanates both from the extracellular space but also from the permeabilized internal stores. On the contrary, in the absence of extracellular calcium the only sources of calcium are the internal organelles. Second, it can be noticed a significantly faster recovery of calcium to pre-pulse levels for the experiments without calcium in the external buffer (compare Figs. 4D and 5D). In the present experiments, the most plausible explanation for the different dynamics observed is the calcium concentration gradient between the cytoplasm and the extracellular space. Under the same pulsing conditions, for experiments in the absence of extracellular calcium the gradient is higher, which makes calcium to diffuse more easily out of the cell through the permeabilized membrane after pulsing. This involves a faster removal of calcium from the cytosol in accordance with a lower measured AUC in the experimental observation time.

3.4. Bipolar square wave permeabilization

Finally, a single bipolar square pulse with the same duration and equivalent V_{RMS} amplitude (reduction by $\sqrt{2}$ factor) was applied for comparison. Experiments were also performed in the presence or absence of external calcium to study separately the permeabilization of the plasma membrane and the internal organelles The goal of these experiments was to study if the use of sine waves provides equivalent permeabilization efficiency than square pulses both in the plasma membrane and internal organelles.

In Fig. 7A the amplitude spectra of the bipolar square pulse and the sine waves were calculated from oscilloscope recordings using a rectangular observation window of 50 ms duration. As observed, the distribution in the frequency content of both type of signals is quite different. As expected, the spectrum of the sine bursts provides single spectral peaks with all the energy concentrated in a very narrow band. On the other hand, the bipolar pulse distributes most of the applied energy around its fundamental frequency but in this case it is significantly widespread. It is interesting to stress that, contrary to unipolar square pulses, the inversing polarity of the square pulses used involves a quasi-zero DC component. In both cases the fact that single bursts were applied prevents the apparition of harmonics associated with the application of trains of repetitive pulses what makes the frequency analysis more precise and simple.

Fig. 7B, C and D (left panels) show the percentages of permeabilization obtained using a single bipolar square pulse for equivalent conditions to the sine waves experiments. In Fig. 7B (5 ms and $E_{peak} = 600/\sqrt{2}$) around 95% of cells displayed the permeabilization of their plasma membrane and this percentage was reduced to 85% for the permeabilization of the internal organelles. In Fig. 7C (5 ms and $E_{peak} = 500/\sqrt{2}$) these values were significantly reduced to around 50% and 40% for the plasma membrane and internal organelles, respectively. Finally, in the last condition (2 ms and $E_{peak} = 600/\sqrt{2}$) the rates of permeabilization in both cases were very similar with a difference of around 5% (values of 72% and 67% respectively).

Comparing to the results obtained with sine waves (depicted in the right panels of Fig. 7) with an $E_{peak} = 600$ V/cm, and regardless the duration, the efficiency of electroporation matches perfectly to the equivalent square pulse condition (Vrms equivalent A/√2) both in the permeabilization of the plasma and internal organelles membranes (Fig. 7B and D). Also the quantification of the AUC provides values similar to those obtained with the lowest frequency sine signal (data not shown). This confirms the proposed equivalence, in the sense of RMS delivered energy, between sine and bipolar square pulses under these conditions. Previous authors explained the equivalence in the electroporation outcomes of different pulse shapes based on the concept of time over the critical threshold [61]. Interestingly, although this previous study did not mention or considered the RMS concept, the analysis of their comparative results between square and sine pulses perfectly follows the rule of RMS equivalence proposed herein.

However, in the present study the results obtained for an $E_{peak} = 500$ V/cm (square RMS value ≈ 350 V/cm) (Fig. 7C) are in clear disagreement with the proposed RMS equivalence. In this last condition, sine waves display a much higher efficiency of permeabilization. The observed mismatch can be explained if we hypothesize that for this condition, the square pulse intensity is near to the critical electroporation value. Under this assumption, the sine wave exceeds this threshold in every cycle, even for a short time, while the square pulse stays around this value (see schematic in Supplementary S2). Consequently, the RMS equivalence is only valid once the electroporation threshold is sufficiently exceeded.

3.5. Theoretical calculations

In order to better understand the results obtained, we made use of a theoretical model to simulate the dependence of the iTMP with the
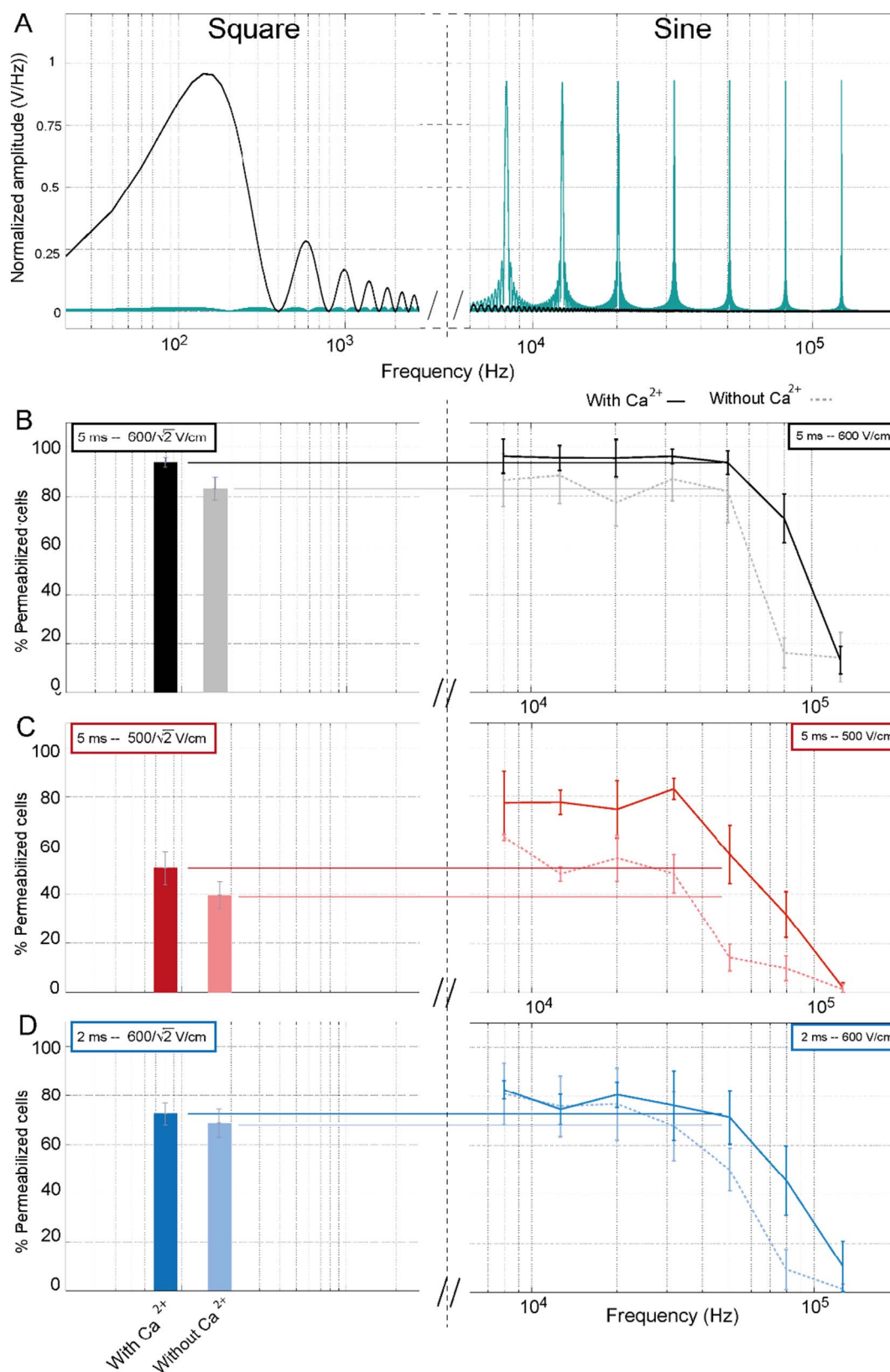
Fig. 7. Bipolar square versus sine wave results. A) Frequency spectra of applied bipolar square pulses (left) and of the sine waves used (right) (x axes are at different scales). Panels B, C and D show the results of the permeabilization rates for each condition assayed for bipolar square pulses (left) and the corresponding sine wave condition (right). Results are shown for experiments with and without calcium. Notice that x axes on left panels B, C and D do not correspond to frequency.

frequency of the applied electric field. The double shell model used provides the values for the external plasma membrane and the internal membrane of a generic organelle. Additionally, the model was computed for different values of membrane conductivity (σ_m) to mimic the different states of electropermeabilization of the external membrane.
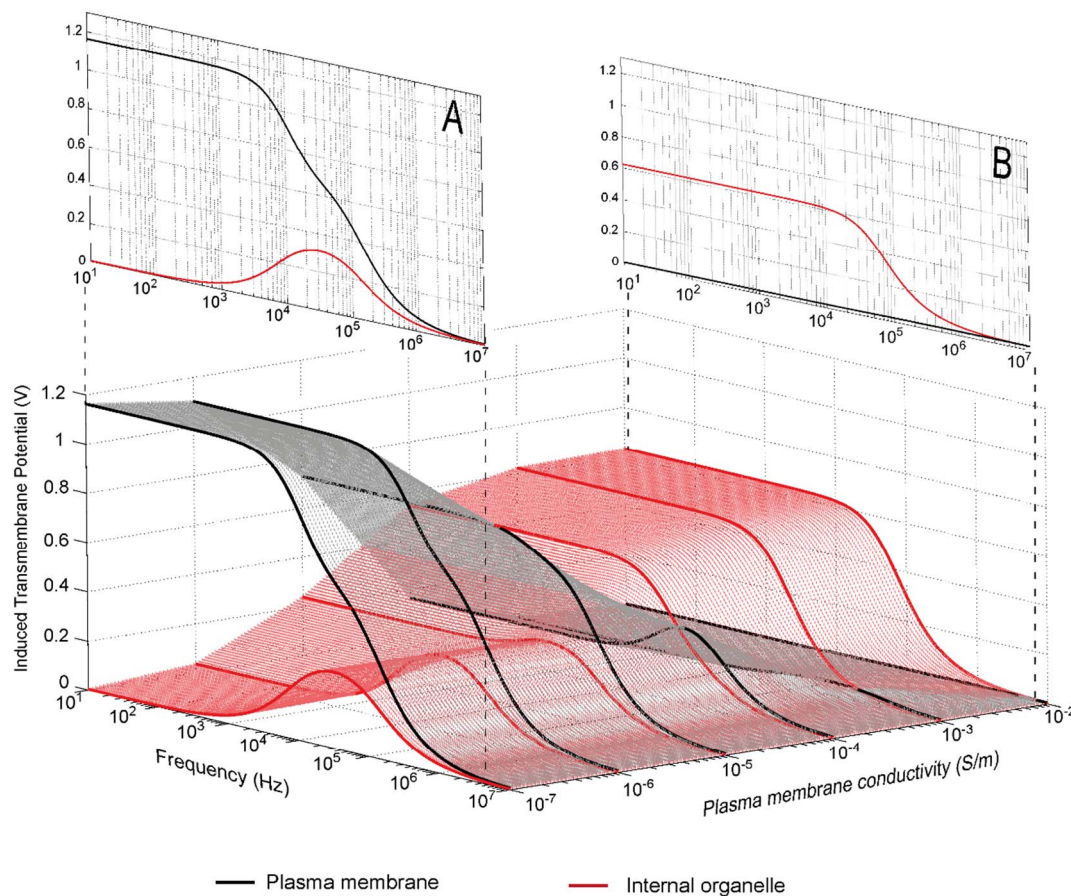
Fig. 8. Computation of the iTMP for both plasma membrane and internal organelle membrane. 3D surface plot depict the calculated iTMP over the frequency for different values of membrane conductivity. Results in insets A and B summarize the values obtained for a membrane conductivity of $\sigma_m = 10-7\,S/m$ and $\sigma_m = 10-2\,S/m$, respectively.

In many theoretical models the membrane conductivity is introduced as a static value corresponding to a nonconductive intact membrane. However, many other studies have experimentally measured and modeled the fact that plasma membrane conductivity rapidly increases by several orders of magnitude upon electroporation [47,62–64]. Especially in our experimental setup, where relatively long duration pulses are applied, this parameter should be treated as dynamically changing during electric field application. For the same cell line used in this study, a recent paper showed the evolution of conductivity during millisecond pulses using the voltage-clamp method [65].

The 3D plot in Fig. 8 shows the results for the evolution in the calculated iTMP for both the plasma membrane (black) and the membrane of an internal organelle (red) for the given frequency range. Notice that the values of the iTMP are in the range usually described for causing cell permeabilization. The results are shown for different values of plasma membrane conductivity (σ_m), while the internal membrane conductivity was fixed to the same value in all simulations. Additional 2D plots for the initial situation, where the conductivity of the plasma membrane is very low ($\sigma_m = 10^{-7}\,S/m$), and for a permeabilized plasma membrane ($\sigma_m = 10^{-2}\,S/m$) are shown in Fig. 8 insets A and B respectively. According to these calculations, the variation of the membrane conductivity in the model clearly influences the frequency response of both external and internal structures. In the initial situation (non-permeabilized membrane), as expected, the outer membrane experiences most of the potential drop across its boundary at low frequency. This value stays in a plateau up to a certain frequency and gradually decreases with increasing frequency producing the well-known low pass filter response of plasma membrane. Under this condition the response of the iTMP in the internal organelle follows a band pass filter behavior with values much lower than for the plasma

membrane. This situation is fully in agreement with the experimental data obtained for the plasma membrane, however, the response for the permeabilization of the internal membranes does not match with our experimental observations.

If we now take into account the changes in plasma membrane due to permeabilization, the previous situation is gradually inversed as the conductivity of the external membrane increases allowing the internal iTMP to reach values over the threshold of permeabilization. It is especially interesting to observe how the frequency response of the internal organelle membrane evolves from a band pass behavior to a low pass response. These results demonstrate how the observed permeabilization in the internal membranes is the result of a two-step process. Once the plasma membrane is permeabilized, it acts no longer as an insulator allowing the electric field to have access to the cell inside. Previous models already proposed this as a mechanism for the manipulation of internal organelles [38]. In the simulation reported here, the frequency-dependent behavior of an internal organelle completely changes from the initially predicted behavior and becomes a low pass filter. The experimental results obtained for the permeabilization of the internal membranes are fully in agreement with this new situation.

The comparison between the frequency response of the plasma membrane and the membrane of the internal structures for the equivalent conditions depicted in Fig. 7 (right panels) still shows some differences. Namely, it can be observed how the cutoff frequency, that is the frequency where the efficiency of permeabilization is drastically reduced, is systematically lower for the internal organelles. For example, in Fig. 7B (right panel) the percentage of cells whose plasma membrane is permeabilized at 80 kHz is around 70% while, under the equivalent condition, only < 20% display permeabilization of the
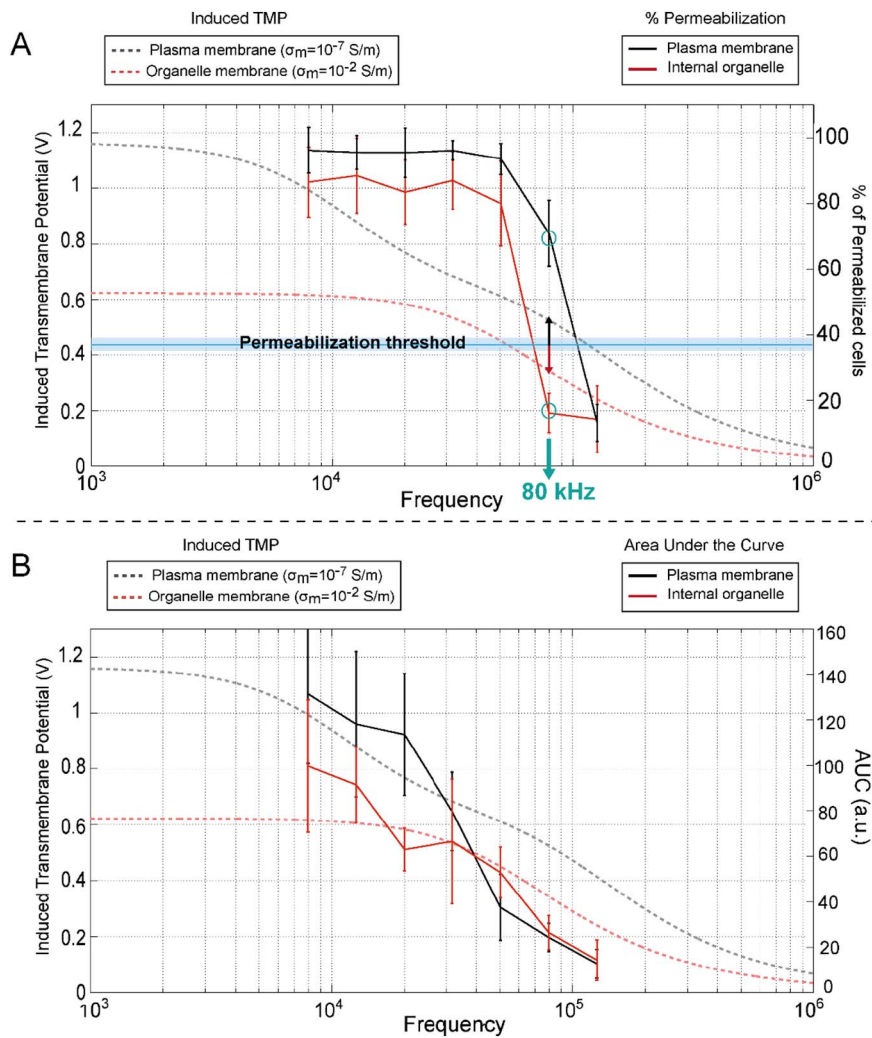
Fig. 9. Comparison between simulation results and corresponding experimental data (5 ms–600 V/cm). Panel A shows the iTMP and % of permeabilization, blue line corresponds to the estimated electroporation threshold. Similarly, panel B shows the iTMP and the AUC quantification for the same condition.

internal organelles. The same behavior is observed for the other two electric field exposure conditions.

To explain this observation, in Fig. 9A the simulation results of the external and the internal iTMP are plotted together for a nonconductive ($\sigma_m = 10^{-7}$ S/m) and a conductive ($\sigma_m = 10^{-2}$ S/m) membrane, respectively. Additionally, the experimental results for the rates of permeabilization of the external and internal membranes for the corresponding simulation parameters (5 ms–600 V/cm) are also depicted in the same figure. It can be observed how the calculated iTMP for an internal organelle displays systematically lower values and a lower cutoff frequency than that of the plasma membrane. Making the assumption that the threshold for permeabilization is similar in both membranes (see blue line in Fig. 9), at low frequencies most of the cells display a calcium spike as the iTMP is above the threshold of permeabilization. However, at a frequency of 80 kHz the predicted iTMP for the plasma membrane stays above the threshold of permeabilization while the value for the internal organelle drops below this threshold (see arrows in Fig. 9A). The results given by the theoretical simulation perfectly describe the experiments observations and justify why a lower cutoff frequency is obtained in the experiments studying the permeabilization of internal organelles.

Nevertheless, there is apparently an important mismatch between the gradual decrease of the calculated iTMP and the steep slope of the experimental data in the frequency band studied. This difference can be explained considering the AUC information. As previously stated, the information provided by the permeabilization rates is the binary response of cells to the electric field (over or under the threshold). By contrast, if the information given by the AUC is used instead (see Fig. 9B), the experimental data perfectly reflect the gradual decrease in the iTMP. These results support the fact that, once the cells are over the threshold of electropermeabilization, a higher value of the iTMP is translated in a higher extent in the modifications produced in the exposed membrane.

Finally, considering the spectral content of square and sine signals (see Fig. 4A), sine waves of the appropriate frequency could be more effective in the permeabilization of the internal organelles (refer to Fig. 8A). Indeed a previous study theoretically suggested that for a certain set of parameters it could be feasible to exceed the iTMP in the internal organelle compared to the plasma membrane [23]. However, our simulations show that if the change in plasma membrane conductivity is considered, the frequency response of the iTMP in the internal organelle completely changes to a situation were similar efficacy should be found for square pulses and sine waves. This theoretical result is confirmed by our experiments.

4. Conclusions

The present paper presents a systematic study of the effects of sine waves in the kHz range on electropermeabilization. Using calcium as a marker of permeabilization it was possible to assess the effects of the AC

electric field on the membranes of cells. Additionally, equivalent square pulses were also used for comparison.

The results for the rates of permeabilization in the plasma membrane show a dependence on the frequency of the sinusoidal electric field according to a low pass filter behavior. This observation is in agreement with the predicted evolution with frequency of the iTMP in the radiofrequency band shown in the simulations. According to our results, the frequency of the sine wave applied could be used as a new tool for controlling electroporation efficiency.

The study of the possible intracellular effects of the electric field reveals also a low pass filter behavior in opposition to classical theoretical predictions that usually assign a band pass behavior. As far as the authors know, this is the first time that the frequency response for the permeabilization of the internal membranes is assessed experimentally. We suggest that the observed results are the result of a two-step process. First, the external membrane is permeabilized and subsequently the internal membrane is affected by the electric field. This hypothesis is confirmed by the simulations considering changes in the conductivity of the plasma membrane.

The comparison in the efficiency of electroporation with bipolar square pulses with amplitude equal to the sinusoidal V_{RMS} values demonstrate equivalent outcomes. This confirms that there is an equivalence in terms of average power applied to the cell membrane between these two signals. In particular, we suggest that this equivalence is only valid if the threshold of permeabilization is exceeded. We propose that the use of sine waves, with a very well-defined narrow frequency band would allow a better uncoupling of the possible different effects of the electric field during electroporation. We think that the use of sine waves should be adopted as a step forward in the understanding of the very complex phenomenon of Electroporation.

Supplementary data to this article can be found online at https://doi.org/10.1016/j.bbamem.2018.01.018.

Transparency document

The Transparency document associated with this article can be found, in online version.

Acknowledgements

References

[1] L.M. Mir, Nucleic acids electrotransfer-based gene therapy (electrogenetherapy): past, current, and future, Mol. Biotechnol. 43 (2009) 167–176, http://dx.doi.org/10.1007/s12033-009-9192-6.

[2] L.M. Mir, S. Orlowski, J. Belehradek Jr., C. Paoletti, Electrochemotherapy potentiation of antitumour effect of bleomycin by local electric pulses, Eur. J. Cancer 27 (1991) 68–72.

[3] R. Heller, R. Gilbert, M.J. Jaroszeski, Clinical applications of electrochemotherapy, Adv. Drug Deliv. Rev. 35 (1999) 119–129, http://dx.doi.org/10.1016/S0169-409X(98)00067-2.

[4] J. Villemejane, L.M. Mir, Physical methods of nucleic acid transfer: general concepts and applications, Br. J. Pharmacol. 157 (2009) 207–219, http://dx.doi.org/10.1111/j.1476-5381.2009.00032.x.

[5] M.P. Rols, Gene transfer by electrical fields, Curr. Gene Ther. 10 (2010) 255.

[6] B. Rubinsky, G. Onik, P. Mikus, Irreversible electroporation: a new ablation modality—clinical implications, Technol. Cancer Res. Treat. 6 (2007) 37–48.

[7] R. Davalos, L. Mir, B. Rubinsky, Tissue ablation with irreversible electroporation, Ann. Biomed. Eng. 33 (2005) 223–231, http://dx.doi.org/10.1007/s10439-005-8981-8.

[8] A. Golberg, M. Belkin, B. Rubinsky, Irreversible electroporation for microbial control of drugs in solution, AAPS PharmSciTech 10 (2009) 881–886, http://dx.doi.

[9] C. Arroyo, J.G. Lyng, Pulsed electric fields in hurdle approaches for microbial inactivation, in: D. Miklavcic (Ed.), Handb. Electroporation, Springer International Publishing, Cham, 2017, pp. 1–30.

[10] K.R. Foster, Thermal and nonthermal mechanisms of interaction of radio-frequency energy with biological systems, IEEE Trans. Plasma Sci. 28 (2000) 15–23, http://dx.doi.org/10.1109/27.842819.

[11] G. Bryant, J. Wolfe, Electromechanical stresses produced in the plasma membranes of suspended cells by applied electric fields, J. Membr. Biol. 96 (1987) 129–139.

[12] R. Hebner, K. Davey, M. Werst, et al., An electromechanical effect on cell membranes, IEEE Trans. Dielectr. Electr. Insul. 24 (2017) 666–674, http://dx.doi.org/10.1109/TDEI.2016.006180.

[13] I. Titushkin, M. Cho, Regulation of cell cytoskeleton and membrane mechanics by electric field: role of linker proteins, Biophys. J. 96 (2009) 717–728, http://dx.doi.org/10.1016/j.bpj.2008.09.035.

[14] T. Kotnik, D. Miklavcic, L.M. Mir, Cell membrane electropermeabilization by symmetrical bipolar rectangular pulses. Part II. Reduced electrolytic contamination, Bioelectrochemistry 54 (2001) 91–95.

[15] R. Ziv, Y. Steinhardt, G. Pelled, et al., Micro-electroporation of mesenchymal stem cells with alternating electrical current pulses, Biomed. Microdevices 11 (2009) 95–101, http://dx.doi.org/10.1007/s10544-008-9213-4.

[16] P. Turjanski, N. Olaiz, F. Maglietti, et al., The role of pH fronts in reversible electroporation, PLoS One 6 (2011) e17303, , http://dx.doi.org/10.1371/journal.pone.0017303.

[17] G. Ruiz, C.J. Felice, Non-linear response of an electrode–electrolyte interface impedance with the frequency, Chaos, Solitons Fractals 31 (2007) 327–335, http://dx.doi.org/10.1016/j.chaos.2005.09.064.

[18] R.W. Glaser, S.L. Leikin, L.V. Chernomordik, et al., Reversible electrical breakdown of lipid bilayers: formation and evolution of pores, Biochim. Biophys. Acta Biomembr. 940 (1988) 275–287.

[19] R.A. Bockmann, B.L. de Groot, S. Kakorin, et al., Kinetics, statistics, and energetics of lipid membrane electroporation studied by molecular dynamics simulations, Biophys. J. 95 (2008) 1837–1850, http://dx.doi.org/10.1529/biophysj.108.129437 (S0006-3495(08)70144-9 [pii]).

[20] J.C. Weaver, Electroporation of biological membranes from multicellular to nano scales, Dielectr. Electr. Insul. IEEE Trans. 10 (2003) 754–768.

[21] J.C. Weaver, K.C. Smith, A.T. Esser, et al., A brief overview of electroporation pulse strength-duration space: a region where additional intracellular effects are expected, Bioelectrochemistry 87 (2012) 236–243, http://dx.doi.org/10.1016/j.bioelechem.2012.02.007.

[22] L.M. Mir, J. Gehl, G. Sersa, et al., Standard operating procedures of the electrochemotherapy: instructions for the use of bleomycin or cisplatin administered either systemically or locally and electric pulses delivered by the CliniporatorTM by means of invasive or non-invasive electrodes, Eur. J. Cancer Suppl. 4 (2006) 14–25, http://dx.doi.org/10.1016/j.ejcsup.2006.08.003.

[23] T. Kotnik, D. Miklavčič, Theoretical evaluation of voltage inducement on internal membranes of biological cells exposed to electric fields, Biophys. J. 90 (2006) 480–491, http://dx.doi.org/10.1529/biophysj.105.070771.

[24] V. Vajrala, J.R. Claycomb, H. Sanabria, et al., Effects of oscillatory electric fields on internal membranes: an analytical model, Biophys. J. 94 (2008) 2043–2052, http://dx.doi.org/10.1529/biophysj.107.114611.

[25] T.R. Gowrishankar, J.C. Weaver, An approach to electrical modeling of single and multiple cells, Proc. Natl. Acad. Sci. 100 (2003) 3203–3208, http://dx.doi.org/10.1073/pnas.0636434100.

[26] S. Katsuki, S. Katsuki, N. Nomura, et al., Biological effects of narrow band pulsed electric fields, IEEE Trans. Dielectr. Electr. Insul. 14 (2007) 663–668.

[27] C. Chen, J.A. Evans, M.P. Robinson, et al., Measurement of the efficiency of cell membrane electroporation using pulsed ac fields, Phys. Med. Biol. 53 (2008) 4747–4757, http://dx.doi.org/10.1088/0031-9155/53/17/019 (S0031-9155(08)79421-1 [pii]).

[28] Y. Zhan, Z. Cao, N. Bao, et al., Low-frequency ac electroporation shows strong frequency dependence and yields comparable transfection results to dc electroporation, J. Control. Release 160 (2012) 570–576, http://dx.doi.org/10.1016/j.jconrel.2012.04.006.

[29] D.C. Chang, P.Q. Gao, B.L. Maxwell, High efficiency gene transfection by electroporation using a radio-frequency electric field, BBA – Mol. Cell Res. 1092 (1991) 153–160, http://dx.doi.org/10.1016/0167-4889(91)90149-R.

[30] D.C. Chang, Cell poration and cell fusion using an oscillating electric field, Biophys. J. 56 (1989) 641–652.

[31] C.B. Arena, M.B. Sano, J.H. Rossmeisl, et al., High-frequency irreversible electroporation (H-FIRE) for non-thermal ablation without muscle contraction, Biomed. Eng. Online 10 (2011) 102, http://dx.doi.org/10.1186/1475-925X-10-102.

[32] S.P. Bhonsle, C.B. Arena, D.C. Sweeney, R.V. Davalos, Mitigation of impedance changes due to electroporation therapy using bursts of high-frequency bipolar pulses, Biomed. Eng. Online (2015), http://dx.doi.org/10.1186/1475-925X-14-S3-S3.

[33] H.P. Schwan, M. Grandolfo, S.M. Michaelson, A. Rindi (Eds.), Biophysics of the Interaction of Electromagnetic Energy With Cells and Membranes, Biol. Eff. Dosim. Nonionizing Radiat. Radiofreq. Microw. Energies, Springer US, Boston, MA, 1983, pp. 213–231.

[34] T. Kotnik, D. Miklavčič, Analytical description of transmembrane voltage induced by electric fields on spheroidal cells, Biophys. J. 79 (2000) 670–679, http://dx.doi.org/10.1016/S0006-3495(00)76325-9.

[35] C. Grosse, H.P. Schwan, Cellular membrane potentials induced by alternating fields, Biophys. J. 63 (1992) 1632–1642, http://dx.doi.org/10.1016/S0006-3495(92)81740-X.

[36] P. Marszalek, D.S. Liu, T.Y. Tsong, Schwan equation and transmembrane potential induced by alternating electric field, Biophys. J. 58 (1990) 1053–1058, http://dx.doi.org/10.1016/S0006-3495(90)82447-4.

[37] E. Tekle, H. Oubrahim, S.M. Dzekunov, et al., Selective field effects on intracellular vacuoles and vesicle membranes with nanosecond electric pulses, Biophys. J. 89 (2005) 274–284, http://dx.doi.org/10.1529/biophysj.104.054494.

[38] A.T. Esser, K.C. Smith, T.R. Gowrishankar, et al., Mechanisms for the intracellular manipulation of organelles by conventional electroporation, Biophys. J. 98 (2010) 2506–2514, http://dx.doi.org/10.1016/j.bpj.2010.02.035.

[39] K.H. Schoenbach, R.P. Joshi, J.F. Kolb, et al., Ultrashort electrical pulses open a new gateway into biological cells, Proc. IEEE 92 (2004) 1122–1136, http://dx.doi.org/10.1109/JPROC.2004.829009.

[40] H.T. Beier, C.C. Roth, G.P. Tolstykh, B.L. Ibey, Resolving the spatial kinetics of electric pulse-induced ion release, Biochem. Biophys. Res. Commun. 423 (2012) 863–866, http://dx.doi.org/10.1016/j.bbrc.2012.06.055.

[41] I. Semenov, S. Xiao, A.G. Pakhomov, Primary pathways of intracellular Ca(2 +) mobilization by nanosecond pulsed electric field, Biochim. Biophys. Acta 1828 (2013) 981–989, http://dx.doi.org/10.1016/j.bbamem.2012.11.032.

[42] G.P. Tolstykh, H.T. Beier, C.C. Roth, et al., Activation of intracellular phosphoi-nositide signaling after a single 600 nanosecond electric pulse, Bioelectrochemistry 94 (2013) 23–29, http://dx.doi.org/10.1016/j.bioelechem.2013.05.002.

[43] C. Dalmay, M.A. De Menorval, O. Français, et al., A microfluidic device with re-movable packaging for the real time visualisation of intracellular effects of nano-second electrical pulses on adherent cells, Lab Chip 12 (2012) 4709, http://dx.doi.org/10.1039/c2lc40857k.

[44] M. Liberti, F. Apollonio, C. Merla, G. D'Inzeo, Microdosimetry in the microwave range: a quantitative assessment at single cell level, IEEE Antennas Wirel. Propag. Lett. 8 (2009) 865–868, http://dx.doi.org/10.1109/LAWP.2009.2028045.

[45] C. Merla, A.G. Pakhomov, I. Semenov, P.T. Vernier, Frequency spectrum of induced transmembrane potential and permeabilization efficacy of bipolar electric pulses, Biochim. Biophys. Acta Biomembr. 1859 (2017) 1282–1290, http://dx.doi.org/10.1016/j.bbamem.2017.04.014.

[46] C. Merla, M. Liberti, F. Apollonio, G. D'inzeo, Quantitative assessment of dielectric parameters for membrane lipid bi-layers from rf permittivity measurements, Bioelectromagnetics 30 (2009) 286–298, http://dx.doi.org/10.1002/bem.20476.

[47] B. Mercadal, P.T. Vernier, A. Ivorra, Dependence of electroporation detection threshold on cell radius: an explanation to observations non compatible with Schwan's equation model, J. Membr. Biol. 249 (2016) 663–676, http://dx.doi.org/10.1007/s00232-016-9907-0.

[48] J. Stratton, Electromagnetic Theory, McGraw Hill, New York, 1941.

[49] T. Kotnik, D. Miklavčič, Theoretical evaluation of the distributed power dissipation in biological cells exposed to electric field, Bioelectromagnetics 21 (2000) 385–394.

[50] H. Hanna, A. Denzi, M. Liberti, et al., Electropermeabilization of inner and outer cell membranes with microsecond pulsed electric fields: quantitative study with calcium ions, Sci. Rep. 7 (2017) 1–14, http://dx.doi.org/10.1038/s41598-017-12960-w.

[51] J.C. Weaver, Electroporation of cells and tissues, Plasma Sci. IEEE Trans. 28 (2000) 24–33.

[52] K.A. DeBruin, W. Krassowska, Modeling electroporation in a single cell. I. Effects of field strength and rest potential, Biophys. J. 77 (1999) 1213–1224, http://dx.doi.org/10.1016/S0006-3495(99)76973-0.

[53] A. Silve, I. Leray, C. Poignard, L.M. Mir, Impact of external medium conductivity on cell membrane electropermeabilization by microsecond and nanosecond electric pulses, Sci. Rep. 6 (2016) 19957.

[54] M. Leguèbe, A. Silve, L.M. Mir, C. Poignard, Conducting and permeable states of cell membrane submitted to high voltage pulses: mathematical and numerical studies validated by the experiments, J. Theor. Biol. 360 (2014) 83–94, http://dx.doi.org/10.1016/j.jtbi.2014.06.027.

[55] S.G. Martinsen, O.G. Martinsen, Bioimpedance and Bioelectricity Basics, Academic Press, San Diego, CA, 2000.

[56] H.P. Schwan, Electrical properties of tissues and cell suspensions: mechanisms and models, Eng. Med. Biol. Soc. 1994. Eng. Adv. New Oppor. Biomed. Eng. Proc. 16th Annu. Int. Conf. IEEE 1 (1994) A70–A71.

[57] M.C. Ashby, V. Tepikin a, ER calcium and the functions of intracellular organelles, Semin. Cell Dev. Biol. 12 (2001) 11–17, http://dx.doi.org/10.1006/scdb.2000.0212.

[58] P.T. Vernier, Y. Sun, L. Marcu, et al., Calcium bursts induced by nanosecond electric pulses, Biochem. Biophys. Res. Commun. 310 (2003) 286–295, http://dx.doi.org/10.1016/j.bbrc.2003.08.140.

[59] G.P. Tolstykh, M. Tarango, C.C. Roth, B.L. Ibey, Nanosecond pulsed electric field induced dose dependent phosphatidylinositol-4,5-bisphosphate signaling and in-tracellular electro-sensitization, Biochim. Biophys. Acta Biomembr. 1859 (2017) 438–445, http://dx.doi.org/10.1016/j.bbamem.2017.01.003.

[60] I. Semenov, S. Xiao, O.N. Pakhomova, A.G. Pakhomov, Recruitment of the in-tracellular Ca2 + by ultrashort electric stimuli: the impact of pulse duration, Cell Calcium 54 (2013) 145–150, http://dx.doi.org/10.1016/j.ceca.2013.05.008.

[61] T. Kotnik, G. Pucihar, M. Reberšek, et al., Role of pulse shape in cell membrane electropermeabilization, Biochim. Biophys. Acta Biomembr. 1614 (2003) 193–200, http://dx.doi.org/10.1016/S0005-2736(03)00173-1.

[62] M. Pavlin, T. Slivnik, D. Miklavcic, Effective conductivity of cell suspensions, IEEE Trans. Biomed. Eng. 49 (2002) 77–80, http://dx.doi.org/10.1109/10.972843.

[63] M. Hibino, M. Shigemori, H. Itoh, et al., Membrane conductance of an electro-porated cell analyzed by submicrosecond imaging of transmembrane potential, Biophys. J. 59 (1991) 209–220, http://dx.doi.org/10.1016/S0006-3495(91)82212-3.

[64] Y. Granot, A. Ivorra, E. Maor, B. Rubinsky, In vivo imaging of irreversible elec-troporation by means of electrical impedance tomography, Phys. Med. Biol. 54 (2009) 4927–4943, http://dx.doi.org/10.1088/0031-9155/54/16/006 (S0031-9155(09)11390-8 [pii]).

[65] L.H. Wegner, W. Frey, A. Silve, Electroporation of DC-3F cells is a dual process, Biophys. J. 108 (2015) 1660–1671, http://dx.doi.org/10.1016/j.bpj.2015.01.038.